

Freeze-thaw effects on pore space and hydraulic properties of compacted soil and potential consequences with climate change

Tobias Klöffel^{*}, Mats Larsbo, Nicholas Jarvis, Jennie Barron

Department of Soil and Environment, Swedish University of Agricultural Sciences, Uppsala, Sweden

ARTICLE INFO

Keywords:

Temperate-boreal zone
Water retention curve
Hydraulic conductivity
Climate change
Sweden
Ultuna

ABSTRACT

Freezing and thawing affect the pore-space structure in agricultural soils with implications for soil hydraulic properties and water flow. Previous studies have focused on the upper few centimeters of the tilled topsoil, where most freeze-thaw (FT) cycles occur, even though deeper soil layers are also subject to freezing and thawing in cold climates. Thus, little is known about how freezing and thawing affect untilled soil layers, which often show high bulk densities that restrict vertical water movement. Furthermore, it remains unclear how shifts in FT patterns with climate change may change the pore-space structure and water flow through these soil layers. Here we investigated the effects of freezing and thawing on X-ray imaged pore-space characteristics, water retention and near-saturated hydraulic conductivity (K) in untilled soil directly below plough depth. Intact cores were sampled at two sites in central Sweden under the same long-term reduced tillage management. The two soils, a silt loam and a silty clay loam, were subjected to three FT scenarios in a laboratory environment intended to represent FT patterns that are considered likely under current and future winter conditions for this region. The latter scenario was characterised by more FT cycles and a lower freezing temperature. Freezing and thawing increased K in the near-saturated range in both soils, which we attribute to observed small ($<0.01 \text{ mm}^3 \text{ mm}^{-3}$) increases in the volume of pores of diameters close to the X-ray resolution limit. Concomitant increases in pore network connectivity and critical pore diameter, especially in the denser silty clay loam soil, probably contributed to this increase in K . The water retention data suggested that changes in pore-space characteristics below X-ray resolution also occurred in both soils. Furthermore, our results indicate that both soils may show higher drainage rates due to shifts in FT patterns in the future, although longer-term changes in pore-space structure with an increasing number of FT cycles would mostly be limited to soils with relatively high clay contents. These soils are often more compacted below plough depth and, thus, benefits from improvements in soil structure such as improved root growth and plant water supply are also expected to be larger.

1. Introduction

Soil structure exerts an important control on water flow and storage in agricultural soils (Jensen et al., 2019; Rabot et al., 2018; Y. Zhang et al., 2022). It is not static, but constantly evolving due to complex interactions of biotic and abiotic processes, in part driven by the climatic boundary conditions of a soil (Bodner et al., 2008; Meurer et al., 2020; Or et al., 2021). One process that is thought to be important for both the inter- and intra-seasonal dynamics of soil structure at higher latitudes and altitudes is freezing and thawing (Bodner et al., 2008; Hirmas et al., 2018). A change in freezing and thawing patterns due to climate warming may thus lead to changes in the dynamics of soil structure with potential implications for soil hydraulic properties and water fluxes.

There is a long history of research on freeze-thaw (FT) effects on soil physical and hydraulic properties. Early works had mostly an “aggregate perspective” (Rabot et al., 2018) looking at properties such as aggregate-size distribution, aggregate stability, mean aggregate diameter and soil erodibility (Bisal and Nielsen, 1964; Bryan, 1971; Dagesse, 2013; Edwards, 1991). By now, the effects of freezing and thawing on these soil physical properties are relatively well understood (e.g., Kværnø and Øygarden, 2006; Ma et al., 2021; Wei et al., 2018). However, pore-space characteristics are clearly better predictors for the hydraulic properties of soils as compared to properties focussing on soil aggregates (Vogel et al., 2022). While many studies have investigated FT effects on soil hydraulic properties such as hydraulic conductivity, infiltration and water holding capacity (Asare et al., 1999; Fouli et al.,

^{*} Correspondence to: Lennart Hjelms väg 9, Uppsala SE-750 07, Sweden.
E-mail address: tobias.kloffel@slu.se (T. Klöffel).

<https://doi.org/10.1016/j.still.2024.106041>

Received 26 October 2023; Received in revised form 24 January 2024; Accepted 8 February 2024

Available online 16 February 2024

0167-1987/© 2024 The Author(s). Published by Elsevier B.V. This is an open access article under the CC BY license (<http://creativecommons.org/licenses/by/4.0/>).

2013; Fu et al., 2019; Unger, 1991), it is only recently that effects on pore-space characteristics have been studied in detail (Taina et al., 2013) and very few of these have quantified pore-space characteristics in tandem with soil hydraulic properties (Leuther and Schlüter, 2021; Liu, Fan, et al., 2021; Liu, Ma, et al., 2021).

The shift in focus away from soil aggregates to pore-space characteristics was triggered by the advent of new imaging technologies, particularly X-ray computed tomography (X-ray CT), which has enabled detailed quantification of the soil pore space (Young et al., 2001). During the last decade, a number of researchers have used X-ray CT to look at FT effects on different pore-space characteristics including macroporosity, pore-size distribution and pore space connectivity (e.g., Leuther and Schlüter, 2021; Liu, Fan, et al., 2021; Miranda-Vélez et al., 2023; Starkloff et al., 2017). These studies exclusively focused on the uppermost soil layer in tilled agricultural topsoils or on repacked soil samples with similar physical conditions (e.g., Liu, Ma, et al., 2021; Starkloff et al., 2017). A focus on the uppermost soil layer makes sense because this is where most FT cycles occur (Henry, 2007). However, soils in the temperate-boreal zone can freeze at greater depth with visible effects on soil structure also in deeper soil layers (Jabro et al., 2014). This is relevant for agricultural soils as they often exhibit a strong reduction in hydraulic conductivity and restricted drainage rates below the depth of tillage as a result of soil compaction (Coquet et al., 2005; Richard et al., 2001; Schlüter et al., 2020; Strudley et al., 2008). Freezing and thawing has been shown to affect the hydraulic properties of agricultural soils and, in particular, to alleviate the effects of soil compaction on hydraulic conductivity (Asare et al., 1999; Jabro et al., 2014; Leuther and Schlüter, 2021; Liu, Fan, et al., 2021; Ma et al., 2019). In addition, the positive effects of freezing and thawing on soil structure in deeper soil layers might be more persistent than in the plough layer since they are not directly affected by soil tillage and the mechanical impact of rain, which can quickly reverse potential benefits (e.g., increased pore connectivity) of freezing and thawing on soil structure (Bryk et al., 2017; Unger, 1991). The lack of understanding of how freezing and thawing affects pore-space characteristics and hydraulic properties below tillage depth is therefore an important knowledge gap.

Freeze-thaw patterns result from the interplay of various factors including air temperature, vegetation cover, soil heat capacity, thermal conductivity, topography, and snow cover (Anderson, 1947; Peng et al., 2017; Sharratt et al., 1992; Shiklomanov, 2012). The latter is considered important since snow can act as an insulation layer that decouples soil and air temperature (Henry, 2007, 2008). Recent studies suggest that a trend towards decreasing snowfall in most parts of Scandinavia, as well as in other parts of the temperate-boreal zone, has already commenced and will likely further intensify in a future climate (Luomaranta et al., 2019; Pulliainen et al., 2020; Quante et al., 2021). This should lead to thinner and more intermittent snow cover, greater fluctuations in soil temperature and thus more frequent FT cycles (Donnelly et al., 2017; Jungqvist et al., 2014; Strandberg et al., 2014). Furthermore, days with temperatures below zero will be increasingly associated with high-pressure systems, which are characterized by a low probability of precipitation (Räisänen, 2016), thus decreasing the likelihood of snowfall and amplifying this trend. However, making detailed projections about how intense these cycles will be is challenging and the subject of ongoing debate. While some studies project that a decrease in the thickness of an insulating snowpack layer, or its complete disappearance, will lead to more intense FT cycles (Decker et al., 2003; Halim and Thomas, 2018), others refer to the simultaneous increase in air temperature and thus expect less intense FT cycles with climate change (Demand et al., 2019; Henry, 2008). These ongoing and projected changes in FT patterns and their consequences for the water functions of agricultural soils have not been explored. However, this knowledge is relevant in the light of expected increases in precipitation in the form of rain during winter in the temperate-boreal zone with climate change (Donnelly et al., 2017; Roudier et al., 2016). In particular, a sufficient permeability of the soil to provide for rapid infiltration and drainage is

required, thereby minimizing the risks of saturated soil conditions, surface runoff and soil erosion. Furthermore, changes in hydraulic functions in response to changing FT patterns may also have consequences for the water supply of plants given the likelihood of an increase in the frequency and severity of spring droughts with climate change in the temperate-boreal zone (Grusson et al., 2021; Spinoni et al., 2018).

The aim of this study was to investigate the effects of freezing and thawing on pore-space characteristics and soil hydraulic properties relevant for soil water functions, in particular drainage and water storage. This was done in a laboratory environment for untilled, compacted agricultural soil, which has so far been neglected despite its relevance in this context. Furthermore, we explored how a change in FT patterns with climate change may affect the pore-space structure and water flow through compacted soil by simulating three contrasting FT scenarios that are considered likely under current and, to the best of our knowledge, future winter conditions in central Sweden.

2. Materials and methods

2.1. Sites and sampling

We sampled soils from a long-term field experiment, which was conducted at two sites in central Sweden located close to each other, Ultuna (59.85°N, 17.64°E) and Säby (59.83°N, 17.70°E). Both soils have been under the same reduced tillage management since 1997, that is, they are chisel ploughed in autumn to a depth of 12 cm and seedbed preparation is performed in spring. The soil at Säby was classified as a Stagnic Phaeozem with a silt loam texture (hereafter referred to as “silt loam”) and the soil at Ultuna is a Eutric Cambisol with a silty clay loam texture (hereafter referred to as “silty clay loam”). Selected soil properties are listed in Table 1.

Soil sampling was conducted on the 2nd of October 2020, which was after chisel ploughing and before the first freezing event (19th of October). Intact soil cores were taken from 12 to 20 cm depth, which is the soil layer directly underlying the ploughed layer. The lack of loosening by tillage at this depth for 23 years, in combination with the regular traffic of machinery has led to compaction of this layer. This is reflected in the high bulk densities, especially in the silty clay loam (Table 1). In total, 24 cores were sampled at each site from within the field plots along a strip ca. 1.5 m from the field margin. Aluminium cylinders (diameter: 6.5 cm, height: 7.5 cm) were greased and inserted into the soil using a falling hammer. Subsequently, the cylinders were gently dug out, tops and bottoms trimmed with a sharp knife and wrapped in plastic foil for transport. Two additional samples per site were taken in the same way and later used for monitoring soil temperatures during the experiment. Finally, disturbed soil for texture and SOC analysis was sampled from the same depth at three locations along the strip. The collected samples were stored in a cold room at 3–4°C until further use.

Table 1

Soil type and soil characteristics of the two sites from the depth of sampling (12–20 cm).

Soil type ^a	Soil texture ^b			Texture class ^a	SOC [%]	Dry bulk density [g cm ⁻³]
	Sand [%]	Silt [%]	Clay [%]			
Stagnic Phaeozem	21	61	18	Silt loam	2.5	1.30 (± 0.03)
Eutric Cambisol	14	51	35	Silty clay loam	1.5	1.63 (± 0.04)

^a Based on IUSS Working Group WRB (2022).

^b Effective particle diameters: Clay: <2 µm; Silt: 2–60 µm; Sand: 60–2000 µm.

2.2. Freeze-thaw scenarios

Three freeze-thaw (FT) scenarios were defined for this laboratory experiment: “Present I”, “Present II” and “Future”. The definitions for the Present I and Present II scenario were based on soil temperature observations during the past 20 years from Ultuna meteorological station, close to the two field sites. During most of these winters within this time period, the soil at 10 cm soil depth either froze only once or did not freeze at all. This is common for relatively cold winters and results mainly from the decoupling of air and soil temperatures due to snow insulation (Henry, 2007; Sharratt et al., 1992). We therefore defined Present I and Present II scenarios as no freezing and one FT cycle respectively. The minimum temperature (T_{\min}) of the Present II scenario was set to -3°C , which is in line with the soil temperature observations.

The Future scenario was derived from climate change projections for central Sweden from the literature. Future winter warming is expected to lead to both air temperatures fluctuating above and below zero degrees more frequently in central Sweden during winter and a decrease in snow depth (Jungqvist et al., 2014; Strandberg et al., 2014; Pulliainen et al., 2020), thereby decreasing the insulation layer between air and soil. As a consequence, FT cycles in the soil are likely to increase. However, uncertainties remain regarding the intensity of future FT cycles in the soil, and therefore the net effect of decreasing snow insulation and increasing winter temperatures (Demand et al., 2019; Henry, 2008). For the Future scenario simulated here, we assumed an increase in freezing intensity and thus lowered T_{\min} to -5°C . Furthermore, we set the number of FT cycles to five, which we assume to be the maximum number of cycles at this soil depth because deeper soil layers freeze less frequently compared with surface soil. The changes in soil structure can be expected to be larger with increasing number of FT cycles and lower freezing temperatures (Li and Fan, 2014). Thus, with this scenario, we assume an “upper possible limit” of changes in soil structure due to freezing and thawing which can be expected with climate change for this region and at this soil depth.

2.3. Laboratory workflow

The laboratory workflow (Fig. 1) is made up of five components: (i) sample preparation, (ii) measurements of pore space characteristics by X-ray CT, (iii) simulation of FT scenarios, (iv) measurement of soil water retention curves, and (v) measurements of infiltration rates in the near-saturated range. The components are described in the following.

2.3.1. Sample preparation

Six samples per soil were randomly assigned to each of the three FT scenarios. All samples, including the ones used for temperature monitoring, were slowly saturated from the bottom for at least two weeks and subsequently drained on a sandbox to a pressure head of -40 cm. This

satisfied the need to reflect the relatively wet soil conditions common during winter, whilst ensuring that pores detectable by X-ray CT would be free of water. The samples were then wrapped in plastic foil to prevent evaporation during the simulation of the FT scenarios. To ensure top-down freezing and thawing, the samples were insulated from the sides using 22 mm-thick pipe insulation (Armaflex AF-4, Ahlsell, Sweden) and from the bottom using 28 mm-thick Styrofoam. Note that, with this setup, the lower boundary conditions of the soil columns do not fully concur with natural winter conditions, where heat and water fluxes directed upwards from deeper soil layers towards the freezing front may occur (Gray and Granger, 1986; Iwata et al., 2010).

2.3.2. X-ray computed tomography

X-ray computed tomography (CT) was used to study changes in different pore-space characteristics induced by freezing and thawing. The samples were scanned with a GE Phoenix X-ray scanner (v|tome|x 240) installed at the Swedish University of Agricultural Sciences in Uppsala, Sweden. We used a voltage of 160 kV and electron fluxes of 500 μA for each sample, and collected 2000 radiographs at an exposure time of 250 ms. The GE image software datos|x 2.1.0 RTM was used to construct 3-D images from the radiographs. With these settings and the given size of the soil cores, we achieved a voxel edge length of 55 μm . X-ray scanning was carried out at different stages of the experiment. In the Present I scenario, the samples were scanned once (after sample preparation). In the other scenarios, the samples were scanned after sample preparation as well as after the last FT cycle. One additional scan was performed for the Future scenario to investigate changes in pore-space characteristics after the first FT cycle (Fig. 1).

Image processing was mainly done using the open-source software ImageJ/FIJI (Schindelin et al., 2012). First, we applied a 3-D median filter with a radius of 2 in all dimensions and an unsharp mask with a radius of 1 and a mask weight of 0.60. The latter was used to sharpen the pore edges. Next, the cores were straightened and moved into the centre of the image canvas. Core walls and the air inside the cylinders served as a basis for normalizing the grey values of the images, which was done using the ImageJ plug-in SoilJ (Koestel, 2018). This allowed us to apply the same grey value threshold to all images for segmentation into binary images. In the next step, we defined cylindrical regions of interest (ROI). For the horizontal direction, the inner diameter of the samples was reduced from 6.5 cm to ca. 5.8 cm (1050 x voxel edge length) for all images. This excluded potential sampling artefacts close to the cylinder walls. To achieve the same for the vertical direction, landmarks (e.g., quartz grains) close to the bottom and top of the samples were identified in all images of the same core and the parts below and above were removed. Although this resulted in slightly differently sized cylindrical ROIs for all images, it enabled us to quantify potential volume changes as a result of freezing and thawing. Since none of the automatic thresholding methods in ImageJ satisfactorily separated pores from the

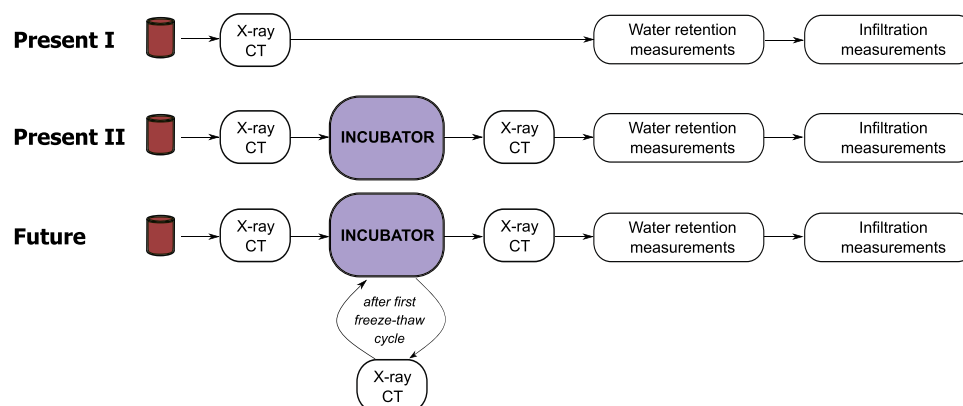


Fig. 1. Workflow for the three freeze-thaw scenarios (Present I, Present II and Future) simulated in this laboratory experiment.

matrix phase, we manually tested different threshold values. A joint histogram, which was calculated for a subset of the images (Koestel, 2018), helped to guide the selection of a threshold that was considered satisfactory for all images. Figure S1 shows one example image for each soil before pre-processing and after segmentation.

Five different pore-space characteristics that are considered relevant for water flow and retention (Schlüter et al., 2020) were calculated from the binary images using SoilJ (Koestel, 2018). We calculated the X-ray-visible porosity, ϕ_{vis} ($\text{mm}^3 \text{mm}^{-3}$), from the ratio between the volume of the cylindrical ROI segmented as pore phase and the total volume of the ROI. Furthermore, the percolating fraction of ϕ_{vis} , F_p (dimensionless), i.e. the fraction of the imaged pore space which is connected to both the upper and lower surfaces of the ROI was determined (Jarvis et al., 2017). As a second indicator for pore space connectivity, we determined the connection probability, Γ (dimensionless), which describes the probability that two random pore voxels in the cylindrical ROI belong to the same pore cluster (Renard and Allard, 2013). The connection probability ranges between 0 and 1, where values approaching 1 indicate a well-connected pore space. Furthermore, we calculated the critical pore diameter, d_c (mm), which is the smallest pore neck of the pore network connecting the upper and lower surface of the ROI (Koestel et al., 2018). Finally, the pore-size distribution (PSD) was determined using the local thickness function implemented in the Python module *PoreSpy* (Gostick et al., 2019) and subsequently normalised by sample volume ($\text{mm}^3 \text{mm}^{-3}$).

2.3.3. Simulation of freeze-thaw scenarios

The FT scenarios were simulated using a cooling incubator (KB Series, BINDER, Germany). For one FT cycle, the incubator was programmed to slowly cool down from a base temperature (T_{base}) of 2°C to T_{min} over two days. Subsequently, the temperature remained at T_{min} for three days to ensure that the samples froze completely. This was confirmed by monitoring the temperatures in the four additional samples (Temperature Probe 107, Campbell Scientific). Finally, the samples were slowly warmed to T_{base} over three days and then remained at T_{base} for a minimum of two days to thaw. The number of FT cycles and T_{min} for the different scenarios are summarized in Table 2.

2.3.4. Soil water retention measurements

For the soil water retention measurements, the cores were first saturated from below, then equilibrated and weighed at eight pressure heads: -10, -30, -50, -100, -300, -600, -1000, and -15000 cm. This was done using sandboxes (-10, -30, -50 and -100 cm; Ejikellkamp), ceramic plates connected to a suction system (-300 and -600 cm) and pressure plate extractors (-1000 and -15000 cm; Soil-Moisture, USA). Water contents at -15000 cm were measured on loose soil. In addition, total soil porosity was derived from dry bulk density and particle density, where the latter was estimated using the pedo-transfer function developed by Schjønning et al. (2017). The water retention measurements were used to estimate the pore-size distribution by translating soil pressure heads to equivalent pore sizes using the Young-Laplace relationship (e.g., Brutsaert, 1966). However, for illustrative purposes, the water retention measurements are also provided in the supplementary material (Figure S2). Note that water retention could not be determined more than once on individual samples as the measurements themselves might cause changes in the pore-space structure.

Table 2
Definition of simulated freeze-thaw scenarios.

Freeze-thaw scenario	Number of simulated freeze-thaw cycles [-]	T_{min} [°C]
Present I	0	-
Present II	1	-3
Future	5	-5

2.3.5. Near-saturated hydraulic conductivity

As a last step, near-saturated hydraulic conductivity (K) was determined for each soil sample at pressure heads of -6 and -1 cm. This was done using mini-disk infiltrometers (METER Group, Germany) with bottom plates of 4.5 cm in diameter leaving space for air to escape at the soil surface. Before the measurements, a thin layer of sand-sized quartz was added onto the surface of each sample to improve the hydraulic contact between infiltrometer and soil. The bottom boundary condition was free drainage. Infiltration was started at a pressure head of -6 cm and continued until at least 30 mL of water had infiltrated as recommended by the manufacturer. Subsequently, the pressure head was increased to -1 cm and the procedure was repeated. Near-saturated K was obtained following the method of Zhang (1997), where the van Genuchten parameters required for this method were estimated from soil texture based on Carsel and Parrish (1988). We note that, due to the low hydraulic conductivities of the compacted soil, the infiltration front at -6 cm pressure head may only have penetrated the upper part of the soil columns and therefore the measurements may not reflect the hydraulic conductivity of the entire soil core. However, at a supply pressure of -1 cm, water was seen to be flowing out of the bottom of all samples, so the measurements will reflect the hydraulic conductivity of the whole soil core. Similar to the water retention measurements, near-saturated K could only be measured once on individual samples for the reasons mentioned above.

2.4. Statistical analysis

In presenting our results, we abstain from null-hypothesis significance testing and the dichotomization of p -values, which is increasingly criticised by the statistical community (e.g., Amrhein et al., 2019; Hector, 2021; Muff et al., 2022; Wasserstein et al., 2019). Instead, we focus on effect sizes. Reporting and discussion of our results are therefore based on point estimates and confidence intervals as a measure of uncertainty (Hector, 2021), presented as arithmetic means and 95% confidence intervals respectively. Furthermore, p -values are discussed in the “language of evidence” as suggested by Muff et al. (2022).

To analyse whether changes in ϕ_{vis} , F_p , Γ and d_c before, during (only Future scenario) and after the FT scenarios were different from zero, we first tested for normality using the Shapiro-Wilk test. The one-sample t -test was used if changes were normally distributed ($p \geq 0.05$) and the Wilcoxon signed-rank test otherwise. With respect to near-saturated K , freezing and thawing increased the variance among the samples in the Present II and Future scenario. Thus, the different FT scenarios were first tested for equal variance using the F -statistic upon which either Student's t -test ($p \geq 0.05$) or Welch's t -test ($p < 0.05$) was used for pairwise comparison. The statistical analysis was performed using the Python module *SciPy* (Virtanen et al., 2020).

3. Results and discussion

3.1. Pore-space characteristics measured by X-ray CT

X-ray-visible porosity, ϕ_{vis} , was larger in the silt loam than the silty clay loam throughout the experiment (Table 3). There was strong evidence that freezing and thawing increased ϕ_{vis} in the silt loam after both FT scenarios, while the evidence was weak (after Present II scenario) to moderate (after Future scenario) in the silty clay loam (Fig. 2). Increases in ϕ_{vis} were on average larger and more variable for the silt loam as evident from the larger point estimates and confidence intervals respectively (Fig. 2; Table S1). Furthermore, all changes in ϕ_{vis} occurred after the first FT cycle in the silt loam, while there was little evidence of further increases in the silty clay loam. Fig. 3 shows that increases in ϕ_{vis} due to freezing and thawing were largely due to increases in the volume of pores with diameters close to the X-ray resolution limit (i.e., 55 μm). In particular, there was strong evidence of increases in pore volume fractions from the resolution limit up to around 0.2 mm pore radius in

Table 3

Mean absolute values of measured pore-space characteristics derived from X-ray CT images. Coefficients of variation (relative standard deviation) are shown in brackets.

Soil	Pore-space characteristic	FT scenario					
		Present I	Present II	Future			
Silt loam	X-ray visible porosity, ϕ_{vis} [$\text{mm}^3 \text{mm}^{-3}$]	0.093 ($\pm 10.1\%$)	0.103 ($\pm 9.1\%$)	0.109 ($\pm 8.8\%$)	0.104 ($\pm 20.0\%$)	0.108 ($\pm 19.5\%$)	0.109 ($\pm 18.8\%$)
	Percolating fraction, F_p [-]	0.87 ($\pm 4.6\%$)	0.89 ($\pm 2.9\%$)	0.90 ($\pm 2.3\%$)	0.87 ($\pm 4.3\%$)	0.87 ($\pm 4.3\%$)	0.87 ($\pm 4.2\%$)
	Connection probability, Γ [-]	0.754 ($\pm 8.9\%$)	0.799 ($\pm 5.7\%$)	0.817 ($\pm 4.7\%$)	0.753 ($\pm 8.6\%$)	0.759 ($\pm 8.6\%$)	0.758 ($\pm 8.4\%$)
	Critical pore diameter, d_c [mm]	0.36 ($\pm 42.4\%$)	0.34 ($\pm 44.2\%$)	0.35 ($\pm 42.9\%$)	0.26 ($\pm 39.2\%$)	0.28 ($\pm 41.2\%$)	0.27 ($\pm 40.9\%$)
	X-ray visible porosity, ϕ_{vis} [$\text{mm}^3 \text{mm}^{-3}$]	0.032 ($\pm 25.3\%$)	0.027 ($\pm 40.4\%$)	0.029 ($\pm 41.7\%$)	0.027 ($\pm 16.8\%$)	0.027 ($\pm 15.2\%$)	0.028 ($\pm 15.8\%$)
Silty clay loam	Percolating fraction, F_p [-]	0.54 ($\pm 55.8\%$)	0.19 ($\pm 149.5\%$)	0.28 ($\pm 102.7\%$)	0.57 ($\pm 47.0\%$)	0.71 ($\pm 14.4\%$)	0.75 ($\pm 9.6\%$)
	Connection probability, Γ [-]	0.453 ($\pm 35.9\%$)	0.454 ($\pm 48.8\%$)	0.468 ($\pm 48.8\%$)	0.478 ($\pm 22.4\%$)	0.521 ($\pm 28.0\%$)	0.565 ($\pm 19.7\%$)
	Critical pore diameter, d_c [mm]	0.67 ($\pm 112.7\%$)	0.41 ($\pm 195.3\%$)	0.45 ($\pm 180.0\%$)	0.31 ($\pm 117.8\%$)	0.38 ($\pm 89.3\%$)	0.38 ($\pm 90.7\%$)
	X-ray visible porosity, ϕ_{vis} [$\text{mm}^3 \text{mm}^{-3}$]	0.032 ($\pm 25.3\%$)	0.027 ($\pm 40.4\%$)	0.029 ($\pm 41.7\%$)	0.027 ($\pm 16.8\%$)	0.027 ($\pm 15.2\%$)	0.028 ($\pm 15.8\%$)
	Percolating fraction, F_p [-]	0.54 ($\pm 55.8\%$)	0.19 ($\pm 149.5\%$)	0.28 ($\pm 102.7\%$)	0.57 ($\pm 47.0\%$)	0.71 ($\pm 14.4\%$)	0.75 ($\pm 9.6\%$)

^a 1st scan: refers to scan before the first freeze-thaw cycle.

^b 2nd scan: refers to scan after the first freeze-thaw cycle.

^c 3rd scan: refers to scan after the last freeze-thaw cycle.

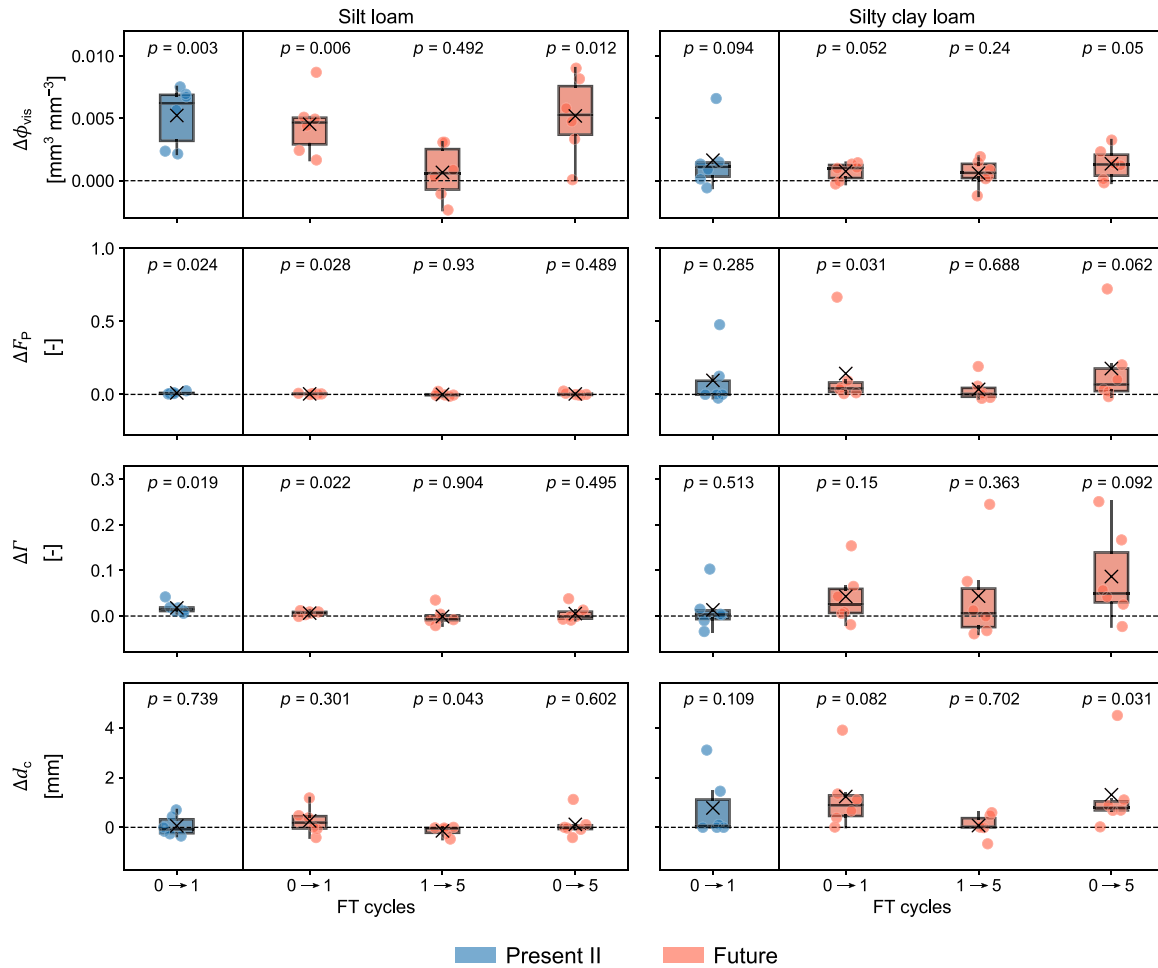


Fig. 2. : Absolute changes (Δ) in X-ray-visible pore-space characteristics measured between different numbers of freeze-thaw (FT) cycles. Crosses and horizontal lines inside the boxplots indicate means and medians respectively; small, transparent dots represent the individual samples. Fliers were removed from the boxplots. ϕ_{vis} : X-ray visible porosity; F_p : percolating fraction of the X-ray visible pore space; Γ : connection probability; d_c : critical pore diameter.

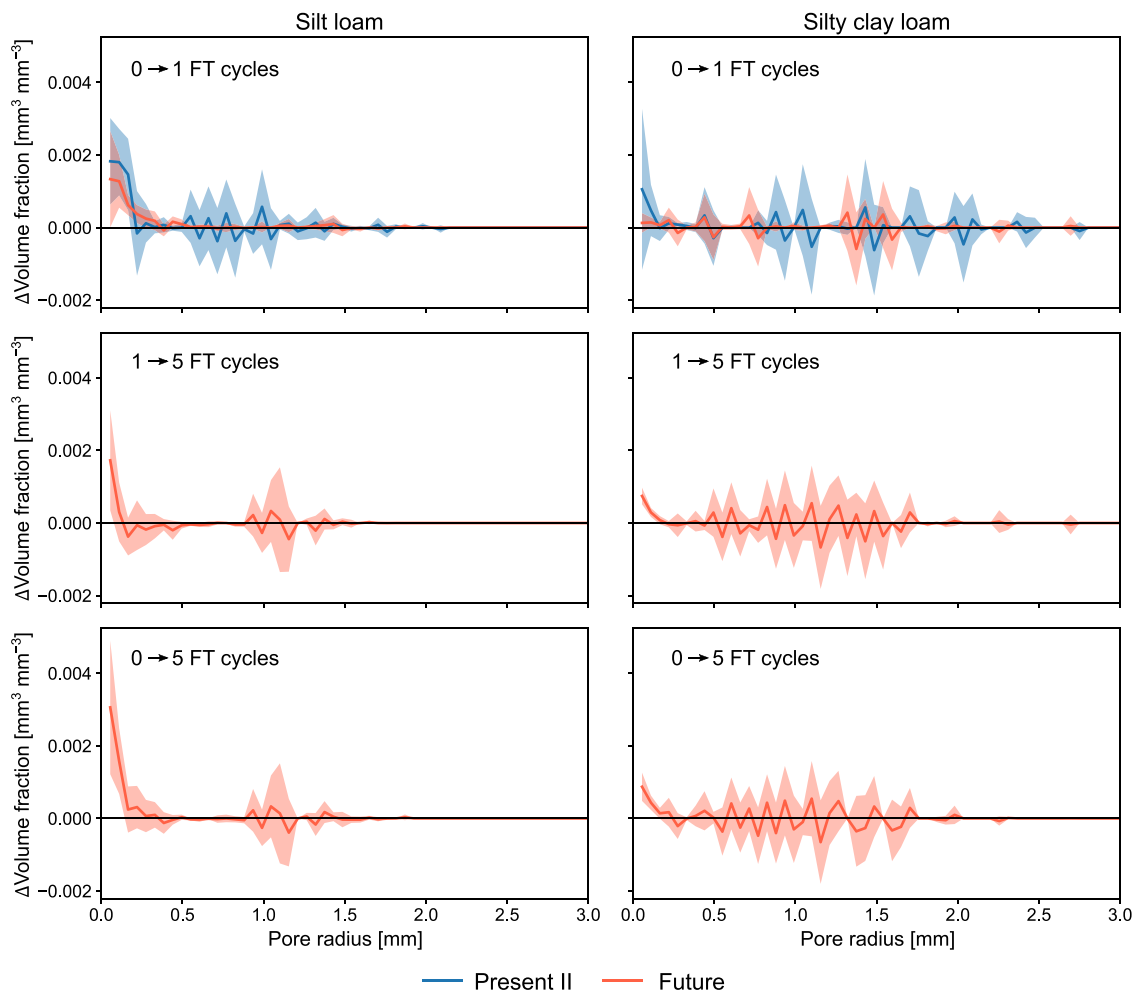


Fig. 3. : Absolute changes (Δ) in pore-volume fractions across pore radii measured by X-ray CT. The figure shows changes after different freeze-thaw (FT) cycles for Present II (blue) and Future scenario (red). Lines and shaded areas indicate arithmetic means and 95% confidence intervals respectively.

the silt loam after the Present II and Future scenario. In the silty clay loam, this was only the case after the Future scenario (Fig. 3). The data suggests that there were additional increases between the first and fifth cycle of the Future scenario in both soils (second row in Fig. 3). Furthermore, changes in pore volume fractions were on average larger and more variable for the silt loam as compared to the silty clay loam after the Future scenario. For pore radii greater than 0.2 mm, both soils showed seemingly random changes.

Our results are in line with Leuther and Schlüter (2021), who reported increases in ϕ_{vis} of a similar magnitude and for pore diameters close to the X-ray resolution limit (X-ray resolution: 48 μm) for an undisturbed silt loam under grassland after 19 FT cycles. In contrast, Miranda-Vélez et al. (2023) found a slight decrease in ϕ_{vis} (X-ray resolution: 58 μm) after five FT cycles for a sandy loam under no-tillage management. A decrease in ϕ_{vis} was also reported by Starkloff et al. (2017) after six FT cycles for a silty clay loam sampled after seedbed preparation (X-ray resolution: 70 μm). Liu et al. (2021) investigated a sieved and re-packed silty clay loam and observed a small increase in ϕ_{vis} (X-ray resolution: 25 μm) of 0.02 $\text{mm}^3 \text{mm}^{-3}$ after five FT cycles. The bulk densities of soils in the above studies were similar to the one of the silt loam in our study. Taken together these results, including the ones of our study, it seems freezing and thawing have limited effects on ϕ_{vis} . The reason for this may be that the X-ray visible pore space is often drained of water prior to freezing (Mohammed et al., 2018), which was also the case in our study. Thus, it might be expected that most effects on soil structure resulting from the expansion of soil water would only be visible close to or below the X-ray resolution limit. It is worth noting that

Leuther and Schlüter (2021) froze their undisturbed grassland samples at -10 hPa matric potential followed by drainage after thawing and still observed only small changes in ϕ_{vis} . However, this might also be related to the increased resilience of grassland soils towards the physical impact of freezing and thawing (Miranda-Vélez et al., 2023). It is also likely that part of the pore space created through the expansion of water due to freezing, in particular horizontal pores (Taina et al., 2013), is re-compressed upon thawing due to gravity, overlaying soil material and matric forces.

The pore connectivity metrics, Γ and F_p , were larger in the silt loam compared with the silty clay loam throughout the experiment, indicating a more connected X-ray visible pore network in the former (Table 3). Fig. 4a shows that there is almost a 1:1 relationship between the square of F_p and Γ for all of the silt loam samples as well as the samples in the silty clay loam with larger X-ray visible porosities. This is an indication that the imaged pore space in these samples is well above the threshold porosity for percolation and is dominated by a single connected percolating pore network (Casali et al., 2023; Jarvis et al., 2017). Several previous studies have demonstrated that the connectivity of X-ray imaged pore networks is strongly determined by the porosity and that these relationships are non-linear, so that at low initial porosities small changes in the pore volume can have considerable effects on pore-space connectivity (Jarvis et al., 2017; Koestel et al., 2018; Lucas et al., 2020; Schlüter et al., 2020). Our data set was no exception, as shown by the relationships in Fig. 4b, c.

There was moderate evidence that freezing and thawing had positive effects on X-ray visible pore space connectivity in the silt loam after both

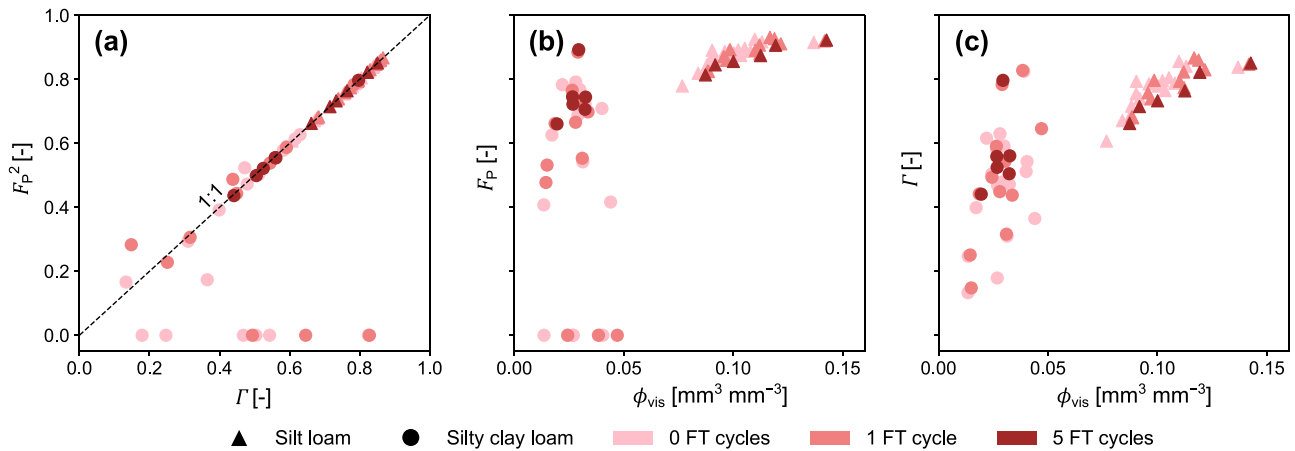


Fig. 4. Relationship between the connection probability (Γ) and the square of the percolating fraction (F_p^2 ; **a**), and the relationship between the two pore connectivity metrics and the X-ray visible porosity (ϕ_{vis} ; **b** and **c**). Data points represent values after different numbers of freeze-thaw (FT) cycles indicated by different colours.

FT scenarios, while there was weak to moderate evidence in the silty clay loam after the Future scenario (Fig. 2). The magnitude and variability of effects differed notably between the two soils, with the silty clay loam showing a relatively large and, for some samples, a quite substantial increase in pore connectivity (Fig. 2; Table S1 and S2). Similarly, Fig. 4b, c illustrate that the visible pore networks in the silty clay loam became more connected after 5 FT cycles since samples with F_p and Γ smaller than 0.4 are no longer present. In contrast, the samples of the silt loam only showed a shift along the x-axis. In other words, although the silt loam showed larger changes in ϕ_{vis} , pore connectivity was more sensitive in the silty clay loam. This is probably because the X-ray visible pore space in the silt loam was initially relatively large and therefore already well-connected (Table 3) so that freezing and thawing hardly showed any positive effects. Finally, it is interesting to note the close relationship between ϕ_{vis} and the connectivity metrics in the silt loam, whereas the relationship is more scattered in the silty clay loam (Fig. 4b, c). This suggests that the samples might have been too small to capture the scale of the pore-space structure in this soil (Jarvis et al., 2017; Koestel et al., 2020).

The critical pore diameter, d_c , was on average larger and much more variable in the silty clay loam than in the silt loam throughout the experiment (Table 3). There was no evidence that freezing and thawing induced any changes in d_c in the silt loam after either Present II or Future scenario, while there was little (Present II scenario) to moderate (Future scenario) evidence for an increase in d_c in the silty clay loam (Fig. 2). In

terms of magnitude, the average increase in d_c in the silty clay loam was slightly larger after the first FT cycle of the Future scenario compared to the Present II scenario (Table S2). However, there was no evidence of further increases in d_c between the first and fifth FT cycle. The likelihood of finding a continuous pathway through a sample with a larger minimum diameter should increase as connectivity improves. In this regard, the difference in response between the two soils makes sense because pore network connectivity was more strongly affected by freezing and thawing in the silty clay loam.

3.2. Soil water retention

The soil water retention measurements revealed no evidence that freezing and thawing had any effects on pore radii $>50 \mu\text{m}$, except for a slight increasing trend in the silt loam. However, freezing and thawing did induce changes in the size distribution of pores below the X-ray resolution limit in both soil types (Fig. 5). For the silt loam, freezing and thawing had a positive effect on the $15\text{--}30 \mu\text{m}$ pore radius range with Future = Present II > Present I. In contrast, there is strong evidence that freezing and thawing had a negative effect on the $1.5\text{--}2.4 \mu\text{m}$ pore radius range after the Future scenario. For the silty clay loam, freezing and thawing had a negative effect in the $2.4\text{--}5 \mu\text{m}$ pore radius range with Present I > Present II > Future. Apart from these changes, Present II and Future scenario had no or no consistent effects (i.e., showing the

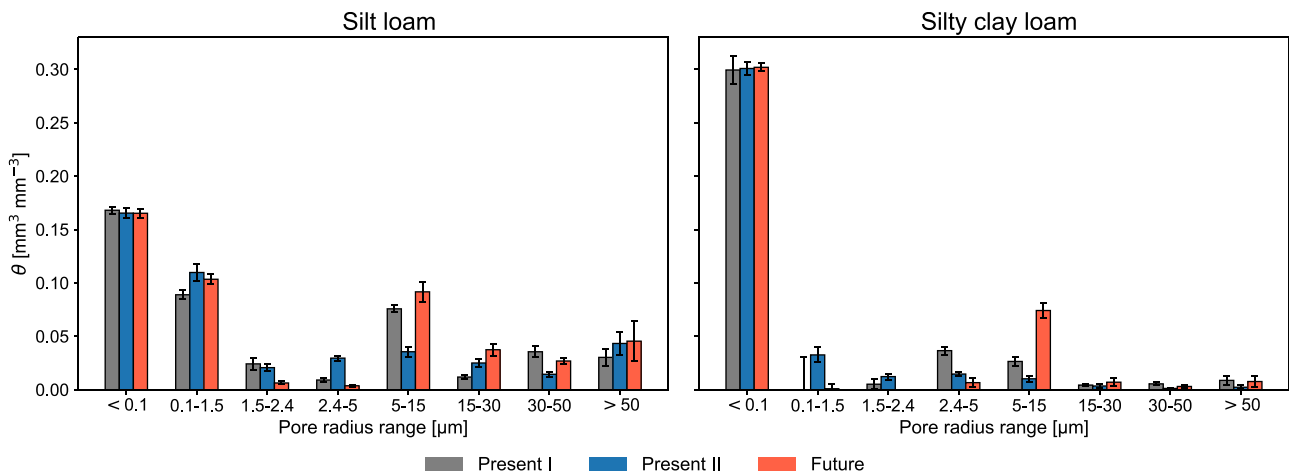


Fig. 5. Pore-size distributions derived from water retention measurements. Pore radii were estimated from the Young-Laplace relationship. Error bars indicate 95% confidence intervals.

same direction of effect) on the pore-size distribution (Fig. 5). However, it is interesting to note the increase in the 5–15 μm pore radius range after the Future scenario, which was evident in both soils and relatively large in the silty clay loam. Our findings are in line with those of Liu et al. (2021) in the sense that these authors also observed continuous and seemingly random modifications of pore-size distributions up to 20 FT cycles. The reason for these shifts in pore-size distribution, however, is not clear. They may be induced by the re-distribution of water within the soil core through repeated freezing and thawing, where water is preferentially transported to locations that freeze first (Koopmans and Miller, 1966; Stähli et al., 1999). The relatively slow freezing and thawing process in this study may have supported this re-distribution. More studies at smaller scales are required to reveal the mechanisms behind changes in pore-size distribution in these pore-size ranges.

3.3. Hydraulic conductivity (K) in the near-saturated range

Hydraulic conductivities in the near saturated range were approximately two orders of magnitude larger at –1 cm than at –6 cm in both soils (Fig. 6), presumably because macropores larger than ca. 250 μm in radius (equivalent to –6 cm pressure head) contributed to water flow. In general, freezing and thawing increased K at both tensions and in both soils. In the silt loam, there was very strong evidence for an increase between Present I and Future, and strong evidence between Present II and Future scenario at –6 cm tension, while at –1 cm tension the evidence was strong between Present I and Present II scenario, and between Present II and Future scenario (Fig. 6). In the silty clay loam, there was strong evidence for an increase between Present I and Future scenario at –6 cm tension, while at –1 cm tension the evidence for an increase was moderate between Present I and Future scenario, and little between Present II and Future scenario. It is important to note that freezing and thawing also increased the spread among the individual samples (see confidence intervals in Fig. 6), indicating that it had relatively large effects on some samples, while it had only small or no effects on others.

Since, at any pressure head, K is mostly determined by the largest water-filled pores, it seems likely that FT effects on near-saturated K in our study may be attributed to the combined effect of observed increases in X-ray visible pore space, network connectivity and critical pore diameter, especially in the silty clay loam (Fig. 2).

We only know of one previous study that has investigated the effects of freezing and thawing on K in the near-saturated range (Fouli et al., 2013), reporting either decreasing or constant infiltration rates at pressure heads of –5 and –10 cm after one and five FT cycles. This is in contrast to our observed increases in K, although clay contents and bulk densities were within the range of our study. This might be because Fouli et al. (2013) used cylinders with repacked soil aggregates that were also drier at the time of freezing (matric potentials smaller than –200 hPa). The latter aspect has not been investigated in the context of pore space characteristics. However, it is known that the water content at the time of freezing is a decisive factor for the effects of freezing and thawing on soil aggregate parameters (Bryan, 1971; Bullock et al., 1988; Li and Fan, 2014). In particular, higher water contents at the time of freezing lead to an increased breakdown of larger into smaller aggregates as more water results in higher destructive forces from the expansion of water. Our results for near-saturated K may also be compared with studies looking at the effects of freezing and thawing on saturated K. However, we only found one study that used *undisturbed* samples (Ma et al., 2019). These authors studied degraded soils with similar textures but lower bulk densities than our soils, reporting increases in K_{sat} of up to two orders of magnitude after 30 FT cycles.

3.4. Implications of climate change for soil structure and soil water functions

Our results suggest that K in the near-saturated range of untilled and compacted soil layers may increase in a future climate with an increasing number of FT cycles and lower freezing temperatures. This is supported by other studies that measured changes in K_{sat} after different

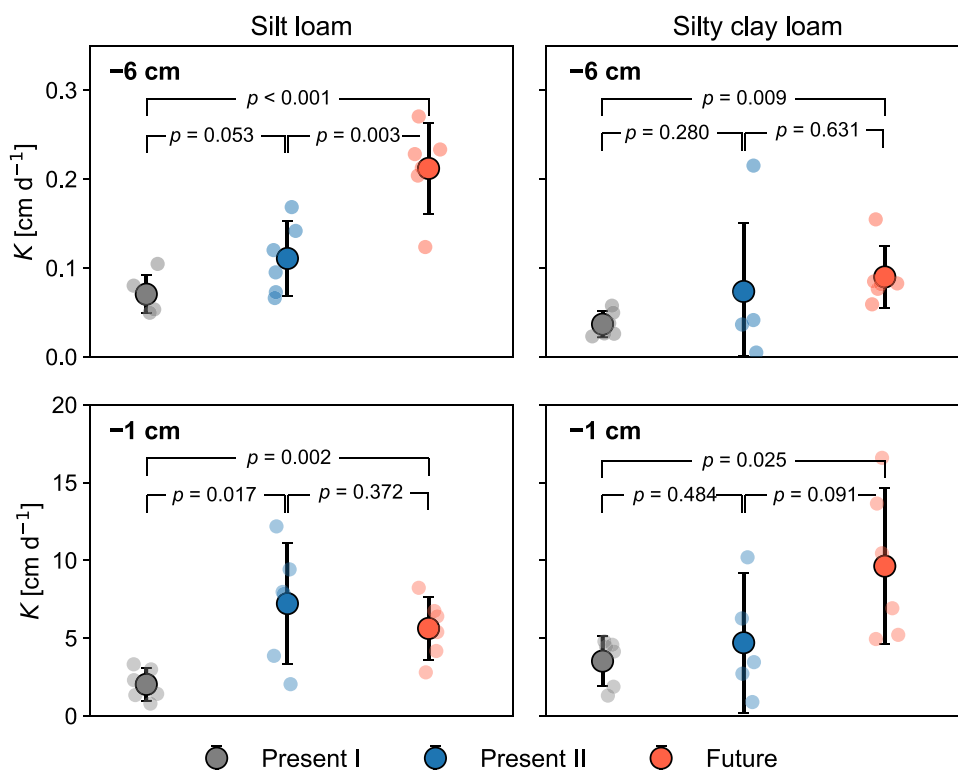


Fig. 6. Hydraulic conductivity (K) in the near-saturated range derived from infiltration measurements at two pressure heads: –6 cm (upper row) and –1 cm (lower row).

numbers of FT cycles (Asare et al., 1999; Ma et al., 2019). Specifically, the data reported by Ma et al. (2019) and Asare et al. (1999), who studied disturbed soils, show that K_{sat} can continue to increase until 5–6 FT cycles for clay loams and silty clay loams, while no further increases, or even decreases, in K_{sat} were found after 1 FT cycle for a silt loam. This pattern is similar to our findings for pore-space characteristics, in particular pore connectivity, and K at a pressure head of -1 cm. In particular, continuous changes with an increasing number of FT cycles were limited to some samples of the silty clay loam in our study. These results indicate that the extent of increases in water flow rates at and very close to saturation with an increasing number of FT cycles may depend on soil type, reaching a maximum earlier (<5 FT cycles) for loamy soils dominated by silt than for soils with higher clay contents. This might be related to the larger cohesive strength of soils with higher clay contents that requires repeated freezing action to be overcome (Bullock et al., 1988). However, the high bulk density of the silty clay loam (Table 1) might have added to this internal resistance towards stresses induced by freezing and thawing. We therefore suggest that soils with high clay contents, which commonly show larger risks of soil compaction and therefore higher bulk densities and smaller macroporosities (Gebhardt et al., 2009; Smith et al., 1997), might particularly respond to shifts in FT patterns.

Considering the overall increase in precipitation expected with climate change for Northern Europe (Gudmundsson and Seneviratne, 2016; Roudier et al., 2016; Strandberg et al., 2014), in particular in the winter, higher K at or near saturation will be beneficial with respect to improved drainage. This is especially true for untilled soil layers below plough depth, which are often compacted and can therefore limit vertical water movement (Coquet et al., 2005; Richard et al., 2001). Furthermore, a better-connected pore system after winter might also benefit root growth in the initial stages of crop growth, especially through untilled and relatively dense soil layers like the silty clay loam in this study (Bengough et al., 2011). Higher pore-space connectivity may also facilitate an improved water supply to plants, which is relevant in the context of spring droughts, which are projected to become more frequent in Sweden in the future (Grusson et al., 2021; Spinoni et al., 2018). However, measurements of unsaturated K across a wider range of pressure heads would be needed to confirm this hypothesis. We know of only one study so far that performed such measurements in relation to freezing and thawing (Leuther and Schlüter, 2021) and which reported increases in unsaturated K for both disturbed and undisturbed soils down to pressure heads of -1000 cm.

4. Conclusions

In this study, we showed that freezing and thawing has the potential to change the pore-space structure and hydraulic properties of untilled and compacted soil layers just below plough depth in fine-textured agricultural soils. Freezing and thawing increased hydraulic conductivity in the near-saturated range of the investigated soil cores, even though absolute changes in X-ray visible porosity were small. In a silty clay loam, this increase in hydraulic conductivity was attributed to increases in the connectivity of X-ray visible pore space and critical pore diameter. Besides this, we found indications that with an increase in the number and intensity of freeze-thaw cycles, as might be expected with climate change in central Sweden, we expect higher soil drainage rates under near-saturated soil conditions and potentially also an improved water supply for plants during spring droughts. Our findings suggest that these positive effects will be more pronounced in soils with higher clay contents, which tend to be more susceptible to compaction and, thus, a change in freeze-thaw patterns with climate change might show larger benefits.

Whether the measured differences in pore-space structure and soil hydraulic properties due to changes in freeze-thaw patterns are of relevant magnitude for the soil water balance and crop growth at field scale and over a whole growing season remains to be investigated.

Furthermore, we note that our findings may only be valid for untilled and compacted soil layers in agricultural soils. Low bulk density soils with a stable and well-developed structure such as under natural grassland or arable soils with a loose and unstable structure after tillage might not show the same response in pore-space characteristics and hydraulic properties towards changes in freeze-thaw patterns. Finally, although the focus of this study is location-specific, we expect these results to be relevant also for other regions in the temperate-boreal zone, which have been experiencing similar decreases in snow depth and thus changes in soil freeze-thaw patterns.

CRedit authorship contribution statement

Klöffel Tobias: Conceptualization, Formal analysis, Methodology, Software, Writing – original draft, Writing – review & editing. **Larsbo Mats:** Methodology, Writing – review & editing, Software. **Jarvis Nicholas:** Supervision, Writing – review & editing. **Barron Jennie:** Conceptualization, Supervision, Writing – review & editing, Funding acquisition.

Declaration of Competing Interest

The authors declare that they have no known competing financial interests or personal relationships that could have appeared to influence the work reported in this paper.

Data Availability

Data will be made available on request.

Acknowledgements

We are grateful to Thomas Keller (Department of Soil and Environment, SLU) and Jumpei Fukumasu (National Agriculture and Food Research Organization, Japan) for their support in the sampling work. Thank you to Anke Herrmann (Department of Soil and Environment, SLU) for providing the cooling incubator and to Wiebke Mareile Heinze (Department of Soil and Environment, SLU) who provided helpful comments on the manuscript. Finally, we thank the Faculty of Natural Resources and Agricultural Sciences (SLU) for financial support of this work.

Appendix A. Supporting information

Supplementary data associated with this article can be found in the online version at [doi:10.1016/j.still.2024.106041](https://doi.org/10.1016/j.still.2024.106041).

References

- Amrhein, V., Greenland, S., McShane, B., 2019. Scientists rise up against statistical significance. *Nature* 567 (7748), 305–307. <https://doi.org/10.1038/d41586-019-00857-9>.
- Anderson, H.W., 1947. Soil freezing and thawing as related to some vegetation, climatic, and soil variables. *J. For.* 45 (2), 94–101.
- Asare, S.N., Rudra, R.P., Dickinson, W.T., Wall, G.J., 1999. Effect of freeze-thaw cycle on the parameters of the green and ampt infiltration equation. *J. Agric. Eng. Res.* 73 (3), 265–274. <https://doi.org/10.1006/jaer.1999.0415>.
- Bengough, A.G., McKenzie, B.M., Hallett, P.D., Valentine, T.A., 2011. Root elongation, water stress, and mechanical impedance: a review of limiting stresses and beneficial root tip traits. *J. Exp. Bot.* 62 (1), 59–68. <https://doi.org/10.1093/jxb/erq350>.
- Bisal, F., Nielsen, K.F., 1964. Soil aggregates do not necessarily break down over-winter. *Soil Sci.* 98 (5), 345–346.
- Bodner, G., Loiskandl, W., Buchan, G., Kaul, H.-P., 2008. Natural and management-induced dynamics of hydraulic conductivity along a cover-cropped field slope. *Geoderma* 146 (1–2), 317–325. <https://doi.org/10.1016/j.geoderma.2008.06.012>.
- Brutsaert, W., 1966. Probability laws for pore-size distributions. *Soil Sci.* 101 (2), 85–92.
- Bryan, R.B., 1971. The influence of frost action on soil-aggregate stability. *Trans. Inst. Br. Geogr.* (54), 71–88.
- Bryk, M., Kołodziej, B., Słowińska-Jurkiewicz, A., Jaroszek-Sierocińska, M., 2017. Evaluation of soil structure and physical properties influenced by weather conditions

- during autumn-winter-spring season. *Soil Tillage Res.* 170, 66–76. <https://doi.org/10.1016/j.still.2017.03.004>.
- Bullock, M.S., Nelson, S.D., Kemper, W.D., 1988. Soil cohesion as affected by freezing, water content, time and tillage. *Soil Sci. Soc. Am. J.* 52 (3), 770–776. <https://doi.org/10.2136/sssaj1988.03615995005200030031x>.
- Carsel, R.F., Parrish, R.S., 1988. Developing joint probability distributions of soil water retention characteristics. *Water Resour. Res.* 24 (5), 755–769. <https://doi.org/10.1029/WR024i05p0755>.
- Casali, E., Larsbo, M., Koestel, J., & Jarvis, N. (2023). *Macropore flow in relation to the geometry and topology of soil macropore networks: Re-visiting the kinematic wave equation* [Submitted to *Journal of Hydrology*].
- Coquet, Y., Vachier, P., Labat, C., 2005. Vertical variation of near-saturated hydraulic conductivity in three soil profiles. *Geoderma* 126 (3–4), 181–191. <https://doi.org/10.1016/j.geoderma.2004.09.014>.
- Dagesse, D.F., 2013. Freezing cycle effects on water stability of soil aggregates. *Can. J. Soil Sci.* 93 (4), 473–483. <https://doi.org/10.4141/cjss2012.046>.
- Decker, K.L.M., Wang, D., Waite, C., Scherbatskoy, T., 2003. Snow removal and ambient air temperature effects on forest soil temperatures in Northern Vermont. *Soil Sci. Soc. Am. J.* 67 (4), 1234–1242. <https://doi.org/10.2136/sssaj2003.1234>.
- Demand, D., Selker, J.S., Weiler, M., 2019. Influences of macropores on infiltration into seasonally frozen soil. *Vadose Zone J.* 18 (1), 1–14. <https://doi.org/10.2136/vzj2018.08.0147>.
- Donnelly, C., Greuell, W., Andersson, J., Gerten, D., Pisacane, G., Roudier, P., Ludwig, F., 2017. Impacts of climate change on European hydrology at 1.5, 2 and 3 degrees mean global warming above preindustrial level. *Clim. Change* 143 (1–2), 13–26. <https://doi.org/10.1007/s10584-017-1971-7>.
- Edwards, L.M., 1991. The effect of alternate freezing and thawing on aggregate stability and aggregate size distribution of some Prince Edward Island soils. *J. Soil Sci.* 42 (2), 193–204. <https://doi.org/10.1111/j.1365-2389.1991.tb00401.x>.
- Fouli, Y., Cade-Menun, B.J., Cutforth, H.W., 2013. Freeze–thaw cycles and soil water content effects on infiltration rate of three Saskatchewan soils. *Can. J. Soil Sci.* 93 (4), 485–496. <https://doi.org/10.4141/cjss2012-060>.
- Fu, Q., Zhao, H., Li, T., Hou, R., Liu, D., Ji, Y., Zhou, Z., Yang, L., 2019. Effects of biochar addition on soil hydraulic properties before and after freezing–thawing. *CATENA* 176, 112–124. <https://doi.org/10.1016/j.catena.2019.01.008>.
- Gebhardt, S., Fleige, H., Horn, R., 2009. Effect of compaction on pore functions of soils in a Saalean moraine landscape in North Germany. *J. Plant Nutr. Soil Sci.* 172 (5), 688–695. <https://doi.org/10.1002/jpln.200800073>.
- Gostick, J., Khan, Z., Tranter, T., Kok, M., Agnaou, M., Sadeghi, M., Jervis, R., 2019. PoreSpy: a python toolkit for quantitative analysis of porous media images. *J. Open Source Softw.* 4 (37), 1296. <https://doi.org/10.21105/joss.01296>.
- Gray, D.M., Granger, R.J., 1986. *In situ* measurements of moisture and salt movement in freezing soils. *Can. J. Earth Sci.* 23 (5), 696–704. <https://doi.org/10.1139/e86-069>.
- Grusson, Y., Westström, I., Joel, A., 2021. Impact of climate change on Swedish agriculture: Growing season rain deficit and irrigation need. *Agric. Water Manag.* 251, 106858. <https://doi.org/10.1016/j.agwat.2021.106858>.
- Gudmundsson, L., Seneviratne, S.I., 2016. Anthropogenic climate change affects meteorological drought risk in Europe. *Environ. Res. Lett.* 11 (4), 044005. <https://doi.org/10.1088/1748-9326/11/4/044005>.
- Halim, M.A., Thomas, S.C., 2018. A proxy-year analysis shows reduced soil temperatures with climate warming in boreal forest. *Sci. Rep.* 8 (1), 16859. <https://doi.org/10.1038/s41598-018-35213-w>.
- Hector, A., 2021. *The New Statistics with R: An Introduction for Biologists* (2nd ed). Oxford University Press. <https://doi.org/10.1093/oso/9780198798170.001.0001>.
- Henry, H.A.L., 2007. Soil freeze–thaw cycle experiments: Trends, methodological weaknesses and suggested improvements. *Soil Biol. Biochem.* 39 (5), 977–986. <https://doi.org/10.1016/j.soilbio.2006.11.017>.
- Henry, H.A.L., 2008. Climate change and soil freezing dynamics: Historical trends and projected changes. *Clim. Change* 87 (3–4), 421–434. <https://doi.org/10.1007/s10584-007-9322-8>.
- Hirmas, D.R., Giménez, D., Nemes, A., Kerry, R., Brunsell, N.A., Wilson, C.J., 2018. Climate-induced changes in continental-scale soil macroporosity may intensify water cycle. *Nature* 561 (7721), 100–103. <https://doi.org/10.1038/s41586-018-0463-x>.
- Iwata, Y., Hayashi, M., Suzuki, S., Hirota, T., Hasegawa, S., 2010. Effects of snow cover on soil freezing, water movement, and snowmelt infiltration: a paired plot experiment, 2009WR008070. *Water Resour. Res.* 46 (9). <https://doi.org/10.1029/2009WR008070>.
- Jabro, J.D., Iversen, W.M., Evans, R.G., Allen, B.L., Stevens, W.B., 2014. Repeated freeze–thaw cycle effects on soil compaction in a clay loam in Northeastern Montana. *Soil Sci. Soc. Am. J.* 78 (3), 737–744. <https://doi.org/10.2136/sssaj2013.07.0280>.
- Jarvis, N., Larsbo, M., Koestel, J., 2017. Connectivity and percolation of structural pore networks in a cultivated silt loam soil quantified by X-ray tomography. *Geoderma* 287, 71–79. <https://doi.org/10.1016/j.geoderma.2016.06.026>.
- Jensen, J.L., Schjønning, P., Watts, C.W., Christensen, B.T., Munkholm, L.J., 2019. Soil Water retention: uni-modal models of pore-size distribution neglect impacts of soil management. *Soil Sci. Soc. Am. J.* 83 (1), 18–26. <https://doi.org/10.2136/sssaj2018.06.0238>.
- Jungqvist, G., Oni, S.K., Teutschbein, C., Futter, M.N., 2014. Effect of Climate change on soil temperature in Swedish boreal forests. *PLoS One* 9 (4), e93957. <https://doi.org/10.1371/journal.pone.0093957>.
- Koestel, J., 2018. SoilJ: An imageJ plugin for the semiautomatic processing of three-dimensional X-ray images of soils. *Vadose Zone J.* 17 (1), 170062. <https://doi.org/10.2136/vzj2017.03.0062>.
- Koestel, J., Dathe, A., Skaggs, T.H., Klakegg, O., Ahmad, M.A., Babko, M., Giménez, D., Farkas, C., Nemes, A., Jarvis, N., 2018. Estimating the permeability of naturally structured soil from percolation theory and pore space characteristics imaged by X-ray. *Water Resour. Res.* 54 (11), 9255–9263. <https://doi.org/10.1029/2018WR023609>.
- Koestel, J., Larsbo, M., Jarvis, N., 2020. Scale and REV analyses for porosity and pore connectivity measures in undisturbed soil. *Geoderma* 366, 114206. <https://doi.org/10.1016/j.geoderma.2020.114206>.
- Koopmans, R.W.R., Miller, R.D., 1966. Soil freezing and soil water characteristic curves. *Soil Sci. Soc. Am. J.* 30 (6), 680–685. <https://doi.org/10.2136/sssaj1966.03615995003000060011x>.
- Kværnø, S.H., Øygarden, L., 2006. The influence of freeze–thaw cycles and soil moisture on aggregate stability of three soils in Norway. *Catena* 67 (3), 175–182. <https://doi.org/10.1016/j.catena.2006.03.011>.
- Leuther, F., Schlüter, S., 2021. Impact of freeze–thaw cycles on soil structure and soil hydraulic properties. *SOIL* 7 (1), 179–191. <https://doi.org/10.5194/soil-7-179-2021>.
- Li, G.-Y., Fan, H.-M., 2014. Effect of freeze–thaw on water stability of aggregates in a black Soil of Northeast China. *Pedosphere* 24 (2), 285–290. [https://doi.org/10.1016/S1002-0160\(14\)60015-1](https://doi.org/10.1016/S1002-0160(14)60015-1).
- Liu, B., Fan, H., Han, W., Zhu, L., Zhao, X., Zhang, Y., Ma, R., 2021. Linking soil water retention capacity to pore structure characteristics based on X-ray computed tomography: Chinese Mollisol under freeze–thaw effect. *Geoderma* 401, 115170. <https://doi.org/10.1016/j.geoderma.2021.115170>.
- Liu, B., Ma, R., Fan, H., 2021. Evaluation of the impact of freeze–thaw cycles on pore structure characteristics of black soil using X-ray computed tomography. *Soil Tillage Res.* 206, 104810. <https://doi.org/10.1016/j.still.2020.104810>.
- Lucas, M., Vetterlein, D., Vogel, H., Schlüter, S., 2020. Revealing pore connectivity across scales and resolutions with X-ray CT. *Eur. J. Soil Sci.* 72 (2), 546–560. <https://doi.org/10.1111/ejss.12961>.
- Luomanta, A., Aalto, J., Jylhä, K., 2019. Snow cover trends in Finland over 1961–2014 based on gridded snow depth observations. *Int. J. Climatol.* 39 (7), 3147–3159. <https://doi.org/10.1002/joc.6007>.
- Ma, Q., Zhang, K., Jabro, J.D., Ren, L., Liu, H., 2019. Freeze–thaw cycles effects on soil physical properties under different degraded conditions in Northeast China. *Environ. Earth Sci.* 78 (10), 321. <https://doi.org/10.1007/s12665-019-8323-z>.
- Ma, R., Jiang, Y., Liu, B., Fan, H., 2021. Effects of pore structure characterized by synchrotron-based micro-computed tomography on aggregate stability of black soil under freeze–thaw cycles. *Soil Tillage Res.* 207, 104855. <https://doi.org/10.1016/j.still.2020.104855>.
- Meurer, K., Barron, J., Chenu, C., Coucheny, E., Fielding, M., Hallett, P., Herrmann, A. M., Keller, T., Koestel, J., Larsbo, M., Lewan, E., Or, D., Parsons, D., Parvin, N., Taylor, A., Vereecken, H., Jarvis, N., 2020. A framework for modelling soil structure dynamics induced by biological activity. *Glob. Change Biol.* 26 (10), 5382–5403. <https://doi.org/10.1111/gcb.15289>.
- Miranda-Vélez, J.F., Leuther, F., Köhne, J.M., Munkholm, L.J., Vogeler, I., 2023. Effects of freeze–thaw cycles on soil structure under different tillage and plant cover management practices. *Soil Tillage Res.* 225, 105540. <https://doi.org/10.1016/j.still.2022.105540>.
- Mohammed, A.A., Kurylyk, B.L., Cey, E.E., Hayashi, M., 2018. Snowmelt Infiltration and macropore flow in frozen soils: overview, knowledge gaps, and a conceptual framework. *Vadose Zone J.* 17 (1), 1–15. <https://doi.org/10.2136/vzj2018.04.0084>.
- Muff, S., Nilsen, E.B., O'Hara, R.B., Nater, C.R., 2022. Rewriting results sections in the language of evidence. *Trends Ecol. Evol.* 37 (3), 203–210. <https://doi.org/10.1016/j.tree.2021.10.009>.
- Or, D., Keller, T., Schlesinger, W.H., 2021. Natural and managed soil structure: On the fragile scaffolding for soil functioning. *Soil Tillage Res.* 208, 104912. <https://doi.org/10.1016/j.still.2020.104912>.
- Peng, X., Zhang, T., Frauenfeld, O.W., Wang, K., Cao, B., Zhong, X., Su, H., Mu, C., 2017. Response of seasonal soil freeze depth to climate change across China. *Cryosphere* 11 (3), 1059–1073. <https://doi.org/10.5194/tc-11-1059-2017>.
- Pulliainen, J., Luojus, K., Derksen, C., Mudryk, L., Lemmetyinen, J., Salminen, M., Ikonen, J., Takala, M., Cohen, J., Smolander, T., Norberg, J., 2020. Patterns and trends of Northern Hemisphere snow mass from 1980 to 2018. *Nature* 581 (7808), 294–298. <https://doi.org/10.1038/s41586-020-2258-0>.
- Quante, L., Willner, S.N., Middelani, R., Levermann, A., 2021. Regions of intensification of extreme snowfall under future warming. *Sci. Rep.* 11 (1), 16621. <https://doi.org/10.1038/s41598-021-95979-4>.
- Rabot, E., Wiesmeier, M., Schlüter, S., Vogel, H.-J., 2018. Soil structure as an indicator of soil functions: A review. *Geoderma* 314, 122–137. <https://doi.org/10.1016/j.geoderma.2017.11.009>.
- Räsänen, J., 2016. Twenty-first century changes in snowfall climate in Northern Europe in ENSEMBLES regional climate models. *Clim. Dyn.* 46 (1–2), 339–353. <https://doi.org/10.1007/s00382-015-2587-0>.
- Renard, P., Allard, D., 2013. Connectivity metrics for subsurface flow and transport. *Adv. Water Resour.* 51, 168–196. <https://doi.org/10.1016/j.advwatres.2011.12.001>.
- Richard, G., Cousin, I., Sillon, J.F., Bruand, A., Guérif, J., 2001. Effect of compaction on the porosity of a silty soil: Influence on unsaturated hydraulic properties. *Eur. J. Soil Sci.* 52 (1), 49–58. <https://doi.org/10.1046/j.1365-2389.2001.00357.x>.
- Roudier, P., Andersson, J.C.M., Donnelly, C., Feyen, L., Greuell, W., Ludwig, F., 2016. Projections of future floods and hydrological droughts in Europe under a +2°C global warming. *Clim. Change* 135 (2), 341–355. <https://doi.org/10.1007/s10584-015-1570-4>.
- Schindelin, J., Arganda-Carreras, I., Frise, E., Kaynig, V., Longair, M., Pietzsch, T., Preibisch, S., Rueden, C., Saalfeld, S., Schmid, B., Tinevez, J.-Y., White, D.J., Hartenstein, V., Eliceiri, K., Tomancak, P., Cardona, A., 2012. Fiji: An open-source platform for biological-image analysis. *Nat. Methods* 9 (7), 676–682. <https://doi.org/10.1038/nmeth.2019>.

- Schjøning, P., McBride, R.A., Keller, T., Obour, P.B., 2017. Predicting soil particle density from clay and soil organic matter contents. *Geoderma* 286, 83–87. <https://doi.org/10.1016/j.geoderma.2016.10.020>.
- Schlüter, S., Albrecht, L., Schwärzel, K., Kreiselmeier, J., 2020. Long-term effects of conventional tillage and no-tillage on saturated and near-saturated hydraulic conductivity – Can their prediction be improved by pore metrics obtained with X-ray CT? *Geoderma* 361, 114082. <https://doi.org/10.1016/j.geoderma.2019.114082>.
- Sharratt, B.S., Baker, D.G., Wall, D.B., Skaggs, R.H., Ruschy, D.L., 1992. Snow depth required for near steady-state soil temperatures. *Agric. For. Meteorol.* 57, 243–251.
- Shiklomanov, N.I., 2012. Non-climatic factors and long-term, continental-scale changes in seasonally frozen ground. *Environ. Res. Lett.* 7 (1), 011003 <https://doi.org/10.1088/1748-9326/7/1/011003>.
- Smith, C.W., Johnston, M.A., Lorentz, S., 1997. Assessing the compaction susceptibility of South African forestry soils. I. The effect of soil type, water content and applied pressure on uni-axial compaction. *Soil Tillage Res.* 41 (1–2), 53–73. [https://doi.org/10.1016/S0167-1987\(96\)01084-7](https://doi.org/10.1016/S0167-1987(96)01084-7).
- Spinoni, J., Vogt, J.V., Naumann, G., Barbosa, P., Dosio, A., 2018. Will drought events become more frequent and severe in Europe? *Int. J. Climatol.* 38 (4), 1718–1736. <https://doi.org/10.1002/joc.5291>.
- Stähli, M., Jansson, P.-E., Lundin, L.-C., 1999. Soil moisture redistribution and infiltration in frozen sandy soils. *Water Resour. Res.* 35 (1), 95–103. <https://doi.org/10.1029/1998WR900045>.
- Starkloff, T., Larsbo, M., Stolte, J., Hessel, R., Ritsema, C., 2017. Quantifying the impact of a succession of freezing-thawing cycles on the pore network of a silty clay loam and a loamy sand topsoil using X-ray tomography. *CATENA* 156, 365–374. <https://doi.org/10.1016/j.catena.2017.04.026>.
- Strandberg, G., Bärring, L., Hansson, U., Jansson, C., Jones, C., Kjellström, E., Kolax, M., Kupiainen, M., Nikulin, G., Samuelsson, P., Ullerstig, A., Wang, S., 2014. CORDEX scenarios for Europe from the Rossby Centre regional climate model. *RCA4 (Rep. Meteorol. Climatol.* 116).
- Strudley, M., Green, T., Ascoughii, J., 2008. Tillage effects on soil hydraulic properties in space and time: state of the science. *Soil Tillage Res.* 99 (1), 4–48. <https://doi.org/10.1016/j.still.2008.01.007>.
- Taina, I.A., Heck, R.J., Deen, W., Ma, E.Y.T., 2013. Quantification of freeze–thaw related structure in cultivated topsoils using X-ray computer tomography. *Can. J. Soil Sci.* 93 (4), 533–553. <https://doi.org/10.4141/cjss2012-044>.
- Unger, P.W., 1991. Overwinter Changes in Physical Properties of No-Tillage Soil. *Soil Sci. Soc. Am. J.* 55 (3), 778–782. <https://doi.org/10.2136/sssaj1991.03615995005500030024x>.
- Virtanen, P., Gommers, R., Oliphant, T.E., Haberland, M., Reddy, T., Cournapeau, D., Burovski, E., Peterson, P., Weckesser, W., Bright, J., van der Walt, S.J., Brett, M., Wilson, J., Millman, K.J., Mayorov, N., Nelson, A.R.J., Jones, E., Kern, R., Larson, E., van Mulbregt, P., 2020. SciPy 1.0: Fundamental algorithms for scientific computing in Python. *Article 3. Nat. Methods* 17 (3) <https://doi.org/10.1038/s41592-019-0686-2>.
- Vogel, H., Balseiro-Romero, M., Kravchenko, A., Otten, W., Pot, V., Schlüter, S., Weller, U., Baveye, P.C., 2022. A holistic perspective on soil architecture is needed as a key to soil functions. *Eur. J. Soil Sci.* 73 (1) <https://doi.org/10.1111/ejss.13152>.
- Wasserstein, R.L., Schirm, A.L., Lazar, N.A., 2019. Moving to a world beyond “ $p < 0.05$ ”. *Am. Stat.* 1–19. <https://doi.org/10.1080/00031305.2019.1583913>.
- Wei, X., Huang, C., Wei, N., Zhao, H., He, Y., Wu, X., 2018. The impact of freeze-thaw cycles and soil moisture content at freezing on runoff and soil loss. *Land Degrad. Dev.*, ldr.3243 <https://doi.org/10.1002/ldr.3243>.
- Young, I.M., Crawford, J.W., Rappoldt, C., 2001. New methods and models for characterising structural heterogeneity of soil. *Soil Tillage Res.* 61 (1–2), 33–45. [https://doi.org/10.1016/S0167-1987\(01\)00188-X](https://doi.org/10.1016/S0167-1987(01)00188-X).
- Zhang, R., 1997. Determination of Soil Sorptivity and Hydraulic Conductivity from the Disk Infiltrometer. *Soil Sci. Soc. Am. J.* 61 (4), 1024–1030. <https://doi.org/10.2136/sssaj1997.03615995006100040005x>.
- Zhang, Y., Weihermüller, L., Toth, B., Noman, M., Vereecken, H., 2022. Analyzing dual porosity in soil hydraulic properties using soil databases for pedotransfer function development. *Vadose Zone J.* 21 (5) <https://doi.org/10.1002/vzj2.20227>.